The dynamics of shear band propagation in metallic glasses

Jian Luo, Liping Huang, Yunfeng Shi*, Binghui Deng*

Department of Materials Science and Engineering,

Rensselaer Polytechnic Institute, Troy, NY 12180, USA

Abstract

Understanding the dynamics of shear band propagation in metallic glasses remains elusive due to the limited temporal and spatial scales accessible in experiments. In micron-scale molecular dynamics simulations on two model metallic glasses, we studied the propagation of a dominant shear band under uniaxial tension with a macroscopic strain of 3-5%. For both materials, the shear band can be intersonic with a propagation speed exceeding their respective shear wave speeds. The propagation exhibits intrinsic instability that manifests itself as microbranching and considerable fluctuations in velocity. The shear strain singularity ahead of propagating shear band tip scales as $1/r$ (r is the distance away from the tip), independent of the macroscopic tensile strain. In addition, we studied the intersection of two shear bands under uniaxial tension, during which path deflection, speed slowing-down, and temperature rise at the junction region were observed. The dynamics of propagating shear band shown here indicate that shear band in metallic glasses can be viewed as shear crack under the framework of weakly nonlinear fracture mechanics theory.

Keywords: metallic glass; shear band propagation; intersonic propagation; shear strain singularity

Correspondence: shiy2@rpi.edu and dengb4@rpi.edu

1. Introduction

Metallic glasses (MGs) are emerging structural materials and possess unique combination of mechanical properties and corrosion resistance [1–3]. Macroscopic metallic glasses normally have a universal yield strain of around 2% at room temperature [4], which is very high as compared to crystalline metal alloys. At micron- or sub-micron scale [5], the yield strain can be further enhanced to 5%, approaching the theoretical limit [6]. One major drawback of metallic glasses is the very limited tensile ductility due to catastrophic failure along a primary shear band. Even for Pd-based metallic glasses with record-breaking toughness, they still fail under tension with nominally zero plasticity along a single shear band [7,8]. Understanding the characteristics of shear band is therefore of key importance to unlock the full potential of metallic glasses in many promising applications.

A shear band in metallic glasses is a thin region with generally nano-meter thickness that localizes plastic deformation [9,10]. The evolution of shear band occurs in three distinct stages: initiation, propagation, and maturation. The first stage is shear band initiation due to structural instability, with or without pre-existing stress concentrators, which could be understood from activity of shear transformation zone (STZ) [11]. The second stage is shear band propagation, generally driven by stored elastic energy, which could interact with other STZs or shear bands [12,13]. The propagation speed is believed to be close to the shear wave speed as demonstrated in a previous molecular dynamics (MD) [14] as well as a mesoscale simulation [15]. The third stage is shear band maturation, during which a dominant across-the-sample shear band continues to glide, leading to local heating or even cavitation and fracture under tension. The speed of gliding during the shear band maturation stage is typically on the order of *mm/s* determined by mechanical

loading conditions and sample dimensions [16], which is much lower than the shear band propagation speed. Due to limitations in temporal and spatial resolution, the second stage of shear band propagation cannot be captured by high-speed camera [16,17] and was only being characterized recently by interrupted compression technique [12,13]. Historically, aligned Eshelby inclusions [18,19], shear crack [20,21] and dislocation [13,22] models have all been proposed to understand the characteristics of shear band propagation, but no consensus has yet been reached. Recent advancement in STZ-vortex mechanism [23,24] in which the Eshelby-like rotation fields generated around STZs will activate the generation of successive STZs in an autocatalytic chain-like manner, has shed new insight into the process of shear band nucleation and propagation. However, it is not fully clear whether the mechanism can accurately predict the shear band propagation speed. Moreover, the dynamics and strain field of a propagating shear band tip remain unresolved, especially under tension.

In this study, we aim to characterize the dynamics of shear band propagation in micron-scale MD simulations, by investigating two well-studied metallic glass systems: a generic binary Lennard-Jones (LJ) glass [25] and a CuZr glass using high-fidelity embedded atom method (EAM) force field [26]. A perturbative static loading (PSL) method [27,28] is used here to circumvent the slow shear band initiation stage, and enable single or multiple shear band propagation across micron-level spatial scale in MD simulations. Our results show that shear band propagation can be intersonic driven by the considerable amount of stored elastic energy for samples under large tensile strain. The shear strain singularity in the vicinity of a running shear band tip is of $1/r$ (r is the distance away from the tip), which is analogous to typical fast running cracks in brittle materials. These findings strongly suggest that the dynamics of shear band propagation in metallic

glasses might well be addressed under the framework of weakly nonlinear fracture mechanics theory [29,30].

2. Simulation methodology

2.1. Sample preparation and simulation setup

The first MG system studied here is a generic binary LJ metallic glass system inspired by Wahnstrom [25] that consists of two equimolar atom species, *S* and *L* for small and large atoms, interacting *via* a binary Lennard-Jones potential of the form:

$$\emptyset(r) = 4\varepsilon_{\alpha\beta}\left(\frac{\sigma_{\alpha\beta}^{12}}{r^{12}} - \frac{\sigma_{\alpha\beta}^{6}}{r^{6}}\right) - \varepsilon_{cutoff} \quad (1)$$

where $\varepsilon_{\alpha\beta}$ and $\sigma_{\alpha\beta}$ (α, β denotes species of *S* or *L*) provide the energy and length scales, respectively. The cutoff $r_{\alpha\beta}^{c}$ is chosen to be species dependent, such that all pair interactions converge to 0.0163 σ_{LL} at the cutoffs of $r_{LL}^{c} = 2.5\sigma_{LL}$, $r_{SL}^{c} = 2.2917\sigma_{LL}$, $r_{SS}^{c} = 2.0833\sigma_{LL}$. The *SS* and *LL* bond energies are equal to that of the *SL* bond energy: $\varepsilon_{SS} = \varepsilon_{SL} = \varepsilon_{LL}$. The *SS* and *SL* length scales are related to the *LL* length scale by: $\sigma_{SS} = 5/6\,\sigma_{LL}$ and $\sigma_{SL} = 11/12\,\sigma_{LL}$. The two atom species have different masses: $m_L = 2m_0$, $m_S = m_0$, where m_0 is mass unit. Accordingly, the internal time scale is $t_0 = \sigma_{LL}\sqrt{m_0/\varepsilon_{LL}}$. In SI units, all the physical quantities follow the conversion in a previous report [31] as: $\sigma_{LL} \approx 2.7$ Å; $m_0 \approx 46$ amu; $\varepsilon_{LL} \approx 0.151$ eV; $t_0 \approx 0.5$ ps.

The second model MG system investigated here is CuZr, which is also an equimolar binary model metallic glass system interacting with a many-body EAM force field that has been well validated against a large set of experimental and *ab initio* data [32,33].

Both the LJ and CuZr metallic glass samples were prepared into thin-slab geometries using conventional melt-quench approach on the platform of LAMMPS [34] package. Temperature and pressure were well-controlled *via* Nose-Hoover [35,36] thermostat and barostat, respectively. Periodic boundary conditions were applied throughout the simulations. The quenching start (T_{high}) and end (T_{low}) temperatures, quenching rate, final sample dimension, density, and elastic properties for both systems are detailed in Table 1. The end temperatures were kept low to reduce thermal noise and the chance of undesired formation of multiple shear bands. Elastic moduli were calculated and averaged with both tension and compression tests in the *x*, *y*, and *z* directions within 1% engineering strain range following our previous study [37].

Table 1. Sample dimension, preparation conditions of the LJ and CuZr model metallic glass systems including the high and low temperatures (T_{high} and T_{low}) as well as the quenching rate ($\dot{Q}$), the Poisson's ratio (v), the Young's modulus (E), the shear modulus (G), the as-quenched glass density (ρ), and the shear wave speed (c_s).

	Dimension (nm^3)	T_{high} (K)	T_{low} (K)	$\dot{Q}$ (K/ps)	v	E (GPa)	G (GPa)	ρ (kg/m^3)	c_s (m/s)
LJ	21.4×2.5×92.1	2000	10	0.087	0.37	67.4	33.7	7454.5	2126.9
CuZr	19.2×1.92×19.2	2500	1	0.1	0.40	62.7	22.4	7281.8	1751.9

2.2. Perturbative static loading test

Typical strain rate accessible in MD simulations is about ten orders magnitude higher than conventional incremental displacement-controlled uniaxial loading test in experiments. Therefore,

one challenge for MD simulation is whether such high strain rate will alter the propagation behavior and dynamics of shear band tip. Moreover, it is known that higher strain rate promotes the formation of multiple shear bands, which could complicate the characterization of shear band propagation dynamics. While one dominant shear band could form in sub-100 nm model system in MD simulations with slower cooling rate and strain rate, and lower deformation temperature [38–42], suppression of multiple shear bands formation in micro-scale samples (with more nucleation sites) may require even slower cooling rate and strain rate, which is computationally inaccessible in microscale MD simulations [43]. To help circumvent these limitations in MD simulations, we employed the PSL method that has been applied to study the local stress state and shear band to cavitation transition during the third stage of shear band maturation or gliding in our previous studies [28]. The essence of the PSL method is to create a slightly weakened region near surface in an loaded sample, which helps nucleate an incipient shear band without excessive waiting time. Subsequently, this shear band propagates into the unperturbed region across the entire sample, providing clean opportunities to study the dynamics and the strain field around a propagating shear band tip. It is worth mentioning that as an alternative to the PSL method, the stress concentrator method by creating a small notch at the sample surface has also been widely used to initiate shear band both in experiments [44] and simulations [23,45,46]. However, the introduction of a small notch in the loaded sample will create a strong and long-range undesired stress distribution, which may complicate the shear band propagation behavior. We therefore proceeded with the PSL method in this study.

As illustrated in Fig. 1, the PSL method essentially consists of sequential operations of elastic loading, replication, perturbation, and static holding. It starts with the as-quenched samples being loaded to various prescribed uniaxial tensile strains (3% to 5%) along *z*-direction under the

plane strain condition with a constant strain rate (0.2 ns^{-1} for the LJ sample, and 0.5 ns^{-1} for the CuZr sample) as rationalized in our previous work [28,47]. Next, the strained samples are replicated (16 by 8 for the LJ system, and 18 by 36 for the CuZr system) to a much larger thin-slab geometry to allow for micron-scale simulation. In addition, two free surfaces (*x*-*y* plane) are created by cutting out a slice (~ 20 nm) parallel to the loading direction to allow shear-offset unconstrainted by the periodic boundary conditions. In the case of 4.5% prescribed uniaxial tensile strain, the final sample size is about 291.4 by 2.5 by 785.5 nm^3 for the LJ system, and 334.9 by 1.92 by 736.4 nm^3 for the CuZr system, respectively. For studies in which longer shear band propagation path is desired (e.g., microbranching, intersonic propagation), the sample width and length is further doubled. To conduct thermal perturbation to initiate the shear band, a prescribed perturbation zone l_p (see Fig. 1) is heated at 2000 K for 5 ps and then relaxed under initial temperature (1 K for the CuZr samples and 10 K for the LJ samples) for another 5 ps. The perturbation zone, tilted at an angle around 48 degrees to the loading direction, is 6 nm in thickness following our previous study [28]. Since shear band propagation is independent of its nucleation [48], this perturbation is expected to have negligible effect on how the shear band propagates. The length l_p of the perturbation zone increases as the uniaxial tensile strain of the sample decreases to ensure that shear band nucleates within reasonable simulation time. The perturbation length l_p is 11 nm for 5% and 4.5% strain, 23 nm for 4% and 3.8% strain, 36 nm for 3.6% strain, and 66 nm for 3.4% and 3.2% strain. We have tested different perturbation lengths under 5%, 4.5%, 4%, 3.8% and 3.6% strain and observed little difference for the shear band propagation speed evolution as demonstrated in Fig. S1 and S2 in the Supplementary Materials.

Lastly, the top and bottom 10 nm portion of the samples along the *z*-direction are clamped and held in place, such that the atoms are free to move perpendicular to the loading direction

(within *x*-*y* plane) but are fixed in the loading direction (*z*-direction). Freezing the holder in *x* and *y* direction would lead to extra shear and bending, while using periodic boundary condition in the loading direction (*z*-direction) will lead to sample rotation. Therefore, the static holding (only along the loading direction with free surfaces) is ideal to drive shear band propagation by the stored elastic energy, under effectively zero macroscopic tensile strain rate. In this way, a shear band is ready to nucleate at the structurally perturbed region under the prescribed tensile strain, then to propagate in the unperturbed region of the sample. The PSL method described here avoids lengthy quenching, elastic loading and shear band nucleation in micron-scale samples.

It is also worth mentioning that strain rate in typical MD simulations is much higher than that in experiments. For this very reason, we choose a loading method with zero strain rate yet with varying initial tensile strain thus different tensile stress. High initial tensile stress in the context of PSL simulations corresponds to high strain rate experiments, or samples with high barriers for shear band nucleation, and *vice versa*. In this regard, the PSL simulations with low initial tensile stress best represent the shear band propagation in typical experiments with low strain rate thus low initial tensile stress. Similarly, observations under high initial tensile stress in the PSL simulations is relevant for experiments under very high strain rates.

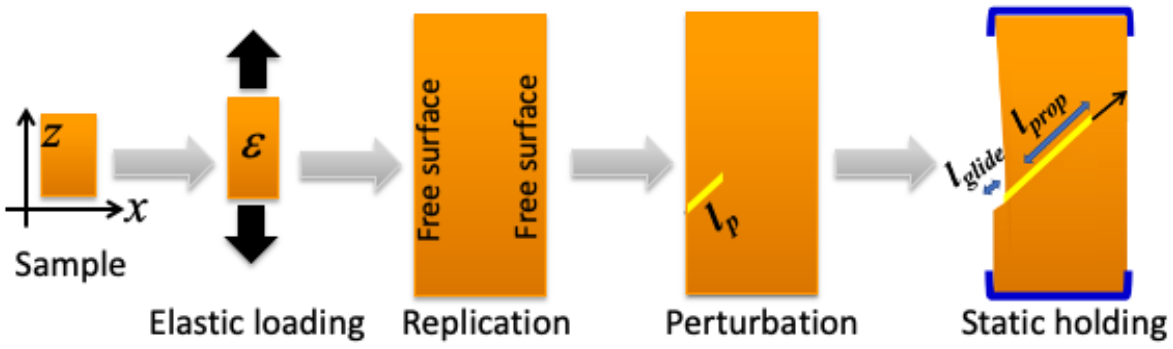

Fig. 1. Schematic of the perturbative static loading test for initiating a single cross-sample shear band and driving its propagation. It involves a sequence of elastic loading, replication, perturbation, and static holding operations. l_p denotes the length of the very initial perturbation. l_{glide} denotes the shear band gliding (shear offset) distance. l_{prop} denotes the shear band propagation distance.

3. Results and discussions

3.1. Shear band propagation speed

In our MD simulations, the shear band tip is monitored by coarse-graining the temperature distribution with 1 nm by 1 nm through-the-thickness griding, as shown in Figure 2(c). The instantaneous shear band position is identified as the farthest grid along the shear band propagation direction with a local temperature rise beyond 50 K. The local temperature is calculated based on the kinetic energy of the atoms in each 1 nm by 1 nm through-the-thickness coarse-grained grid. It should be noted that, as the shear band propagates across the entire sample in Figure 2(c) over a distance ~280 nm, while the shear offset (or shear band gliding) on the left surface is only about 12 nm. Therefore, the shear band propagation speed is close to 1000 m/s, while the shear band gliding (shear offset) speed is only around 24 m/s.

Fig. 2 shows the shear band tip position as a function of time, as well as the average shear band propagation speed for the LJ system under different prescribed uniaxial tensile strains. Within the 1 ns time span accessible in our simulation, shear band propagation was observed when the tensile strain is larger than 3%. The average propagation speed near the center of the sample

increases monotonically with the prescribed uniaxial tensile strain. Importantly, the shear band propagation speed surpasses the shear wave speed for sample with prescribed uniaxial tensile strain of 5%.

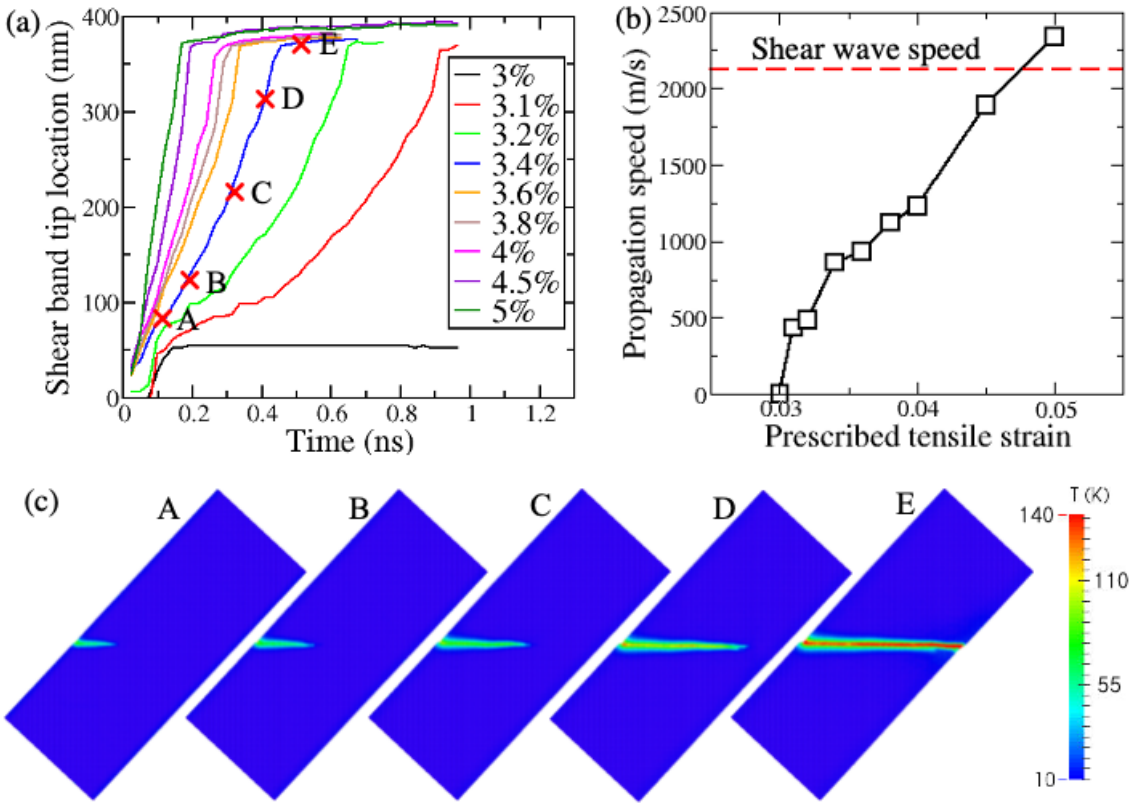

Fig. 2. (a) Temporal evolution of shear band propagation in LJ samples under different prescribed tensile strains. (b) The corresponding average shear band propagation speed by linearly fitting the steady propagation region near the center of the sample between 150 nm and 250 nm. (c) Representative snapshots of shear band propagation at simulation running time of 0.1, 0.2, 0.3, 0.4, and 0.5 ns for the LJ sample with 3.4% prescribed tensile strain as marked by the red crosses in (a).

As the shear band propagates with a varying speed, it is also important to examine how the instantaneous shear band propagation speed evolves over time. Fig. 3 shows the instantaneous shear band propagation speed normalized by the shear wave speed (c_s) for both the LJ samples and the CuZr samples under different prescribed tensile strains. It can be seen that the shear band propagation speed fluctuates substantially, which is similar to experimental observation of crack propagation in polyacrylamide gel and soda-lime glass [49,50]. The fluctuation is probably due to both the intrinsic shear band instability as well as local structural heterogeneity of the glassy sample as evidenced in many studies [24,46,51,52]. For the LJ sample, under 3.2% prescribed uniaxial tensile strain, the shear band propagation is marginally sustainable with momentary stoppage after running for 50 nm and 70 nm. The shear band propagation speed varies from 0.2 c_s to 0.5 c_s. Under 4.5% prescribed uniaxial tensile strain, the shear band accelerates to 0.5 c_s and stays at 0.5 c_s within the first 200 nm of propagation. Subsequently, the shear band advances at c_s for about 100 nm and slows down again. Finally, the shear band accelerates and stays above c_s for 200 nm distance towards the end. Under 5% prescribed uniaxial tensile strain, the shear band propagation speed increases and fluctuates at around c_s for the first 400 nm with momentarily reaching $\sqrt{2}c_s$, which is the forbidden velocity for steady-state non-radiative dislocations found by Eshelby [53].

The shear band propagation in the CuZr samples is quite similar to that in the LJ samples: (1) The average speed of shear band propagation increases with increasing prescribed uniaxial tensile strain; (2) The instantaneous speed of shear band propagation increases with time in general yet with significant fluctuations; (3) The shear band can travel faster than the shear wave, particularly for the CuZr sample with 5% prescribed uniaxial tensile strain.

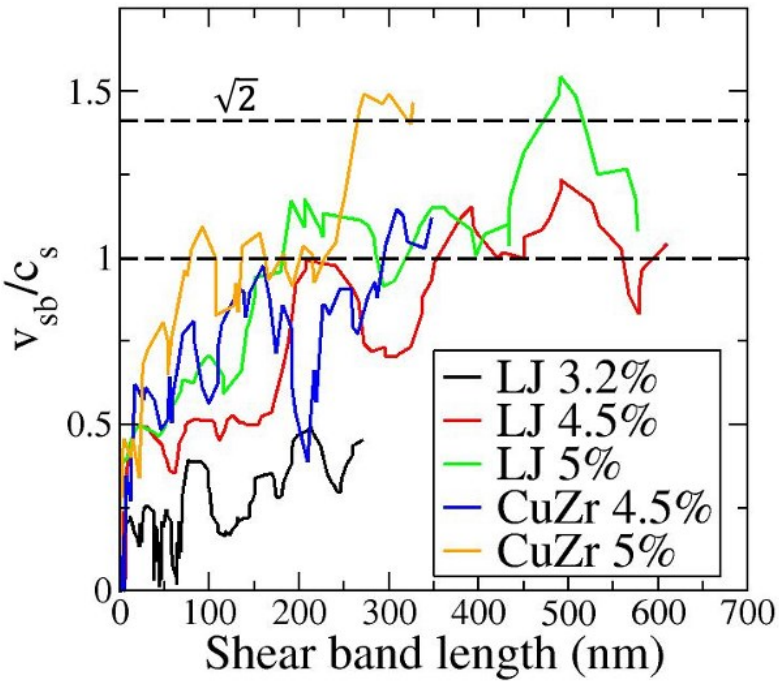

Fig. 3. Instantaneous shear band propagation speed (fitted over 5 ps duration) normalized by shear wave speed as a function of real time shear band length for the LJ sample and CuZr sample under different prescribed uniaxial tensile strains. The associated velocity measurement uncertainty is estimated to be around 100 m/s (~ 0.05 c_s for the LJ samples and ~ 0.06 c_s for the CuZr samples).

3.2. Shear strain distribution and singularity

Fig. 4 shows the shear strain distribution at different simulation times for a LJ sample under 4.5% prescribed uniaxial tensile strain. The shear band region exhibits a negative ε_{zx}, while the region on both sides of the shear band elastically unloads thus exhibiting a positive ε_{zx}. The shape of the elastically unloading regime evolves as the shear band propagates and accelerates. After 0.34 ns, the front of the elastically unloading regime resembles a Mach cone behind the shear band tip, consistent with a propagating speed that is higher than the shear wave. This is surprising according to the continuum mechanics in which the Rayleigh wave speed should be the terminal

speed for shear crack under mode II shear loading [54–56]. Complications at the propagation front such as the nonlinearity [29,30] may give rise to the intersonic propagation behavior. Given that intersonic propagation has also been observed in many other systems, such as cracks [55,56], twinning [57,58], dislocation [59–61] and shear rupture during earthquakes [62], the new observations thereof indicate that the intersonic propagation might be quite general for shear dominated deformations in solids.

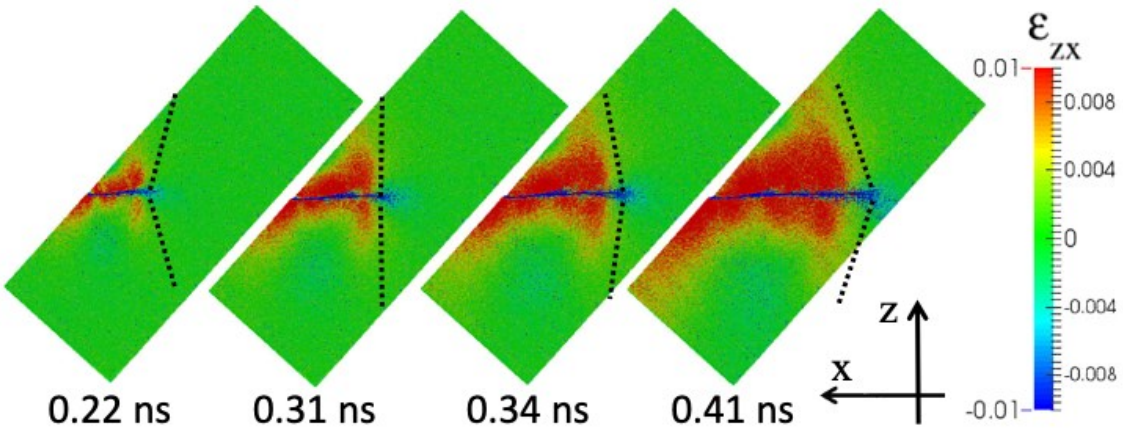

Fig. 4. Shear strain field evolution for a 0.58 μm by 1.57 μm LJ sample under prescribed uniaxial tensile strain of 4.5%. The Mach cone after 0.34 ns clearly demonstrates that the shear band propagation speed is larger than the shear wave speed. The local shear strain field is calculated over the 1 nm by 1 nm through-the-thickness grid using the affine deformation matrix that best fits the deformation from the initial atomic configuration to the current atomic configuration [11].

To further reveal the nature of shear band propagation, we also characterized the shear strain singularity ahead of the propagating shear band tip as shown in Fig. 5. The atomic shear strain was calculated using the initial state of static holding as the reference. In both the LJ system and the CuZr system under different prescribed uniaxial tensile strains, the shear strain ahead of the shear band tip scales in a $1/r$ relationship, where r is the distance away from the shear band tip

in the propagating direction. This is surprising and in stark contrast with the well-known linear elastic fracture mechanics (LEFM) where strain field ahead of a crack tip exhibits a $1/\sqrt{r}$ relationship. Interestingly, the $1/r$ strain singularity observed here is in agreement with the characteristics of the near-tip strain field of rapidly moving cracks as demonstrated in many studies under the framework of recently developed weakly nonlinear fracture mechanics theory [29,30]. Specifically, Livne and coworkers [63,64] recently showed that the LEFM will break down near the crack tip at high propagation speed and the strain field follows $1/r$ relationship due to the violation of the small strain assumption. Given that the speed of shear band propagation is indeed very fast as shown in Fig. 3, and the stress-strain curve of a metallic glass sample is clearly nonlinear beyond 2% macroscopic strain as commonly observed in simulations [65,66] and experiments [6,67], the $1/r$ shear strain field observed here, therefore, suggests that the nature of shear band propagation dynamics might be interpreted as a rapidly moving shear crack with weak nonlinearity near the tip.

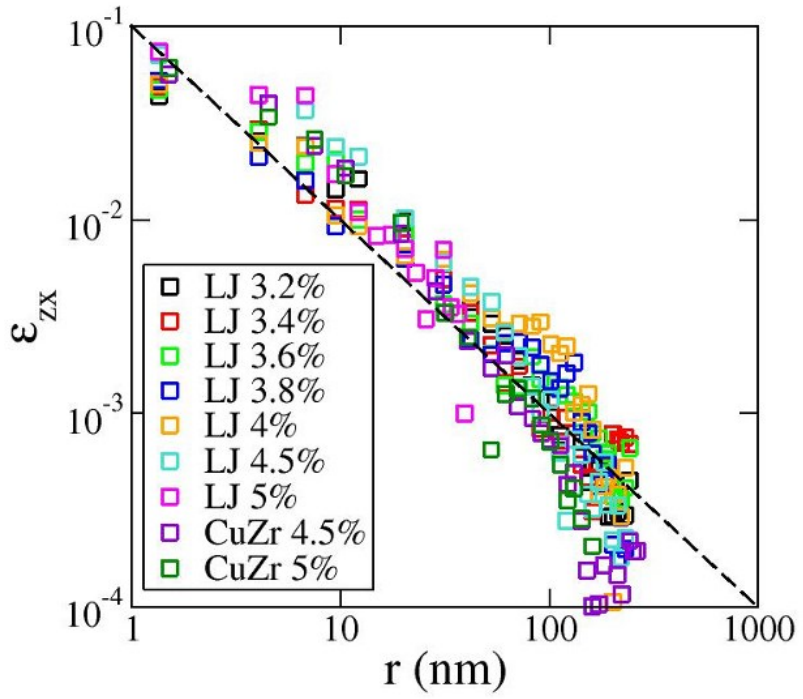

Fig. 5. Shear strain as a function of distance ahead of the shear band tip in the LJ samples and CuZr samples under different prescribed uniaxial tensile strains. The dashed black line has a slope of -1 in this log-log plot, indicating $\varepsilon_{zx} \propto 1/r$.

3.3. Dynamic instability of propagating shear band

The intersonic shear band propagation speed, together with the $1/r$ shear strain singularity ahead of shear band tip strongly suggest that the dynamics of rapidly propagating shear band might share the same mechanics with that of shear crack under the framework of weakly nonlinear elastic fracture mechanics theory. Crack in brittle materials typically does not always propagate *via* individual straight path, but either microscopically branches or spontaneously oscillates when the speed is sufficiently high [68,69], unless it is purposely suppressed in an engineering way as demonstrated in many studies [70,71]. Therefore, it is expected that shear band propagation also

exhibits intrinsic dynamic instabilities due to the resemblance between traveling shear band and shear crack.

Fig. 6 shows some representative moments when the propagating shear band tip branches in the large LJ sample with 4.5% prescribed uniaxial tensile strain. The shear band is clearly depicted by the temperature field. Particularly, it takes about 200 nm for the first branching event to occur, which roughly coincides with the moment when the shear band propagation speed gets close to the shear wave speed as shown in Fig. 3. Afterwards, another branching event appears as the tip picks up propagation speed again. The repetitive branching events lead to considerable fluctuations of the instantaneous traveling speed of shear band tip. In addition, the temperature rise in the shear band is not homogeneous with the tail being hotter than the tip. This is consistent with the accumulative buildup of the displacement as the sample continues to slide along the shear band as shown in Fig. S3 in the Supplementary Material. Overall, the branching behavior of the propagating shear band exhibits a striking resemblance with that of other typical rapidly moving crack scenarios [72–75], further suggesting that the nature of shear band tip can be viewed as a shear crack tip.

The atomic mechanism of shear band branching and multiplication has been thoroughly investigated recently. Essentially, the shear banding process in a homogeneous metallic glass is believed to be based on the autocatalytic generation of successive STZs and vortex-like rotation fields, leading to STZ percolation and, ultimately, to the formation of a shear band [23]. The branching behavior could be trigged whenever the STZ-vortex mechanism is considerably perturbed either by structural heterogeneities [45] or stress fluctuations [76]. Even though the atomic structure of metallic glasses is highly heterogeneous [46,51], we believe that the shear band

branching behavior observed here was mainly ascribed to the typical intrinsic propagation instability at high speed, over which stage most branching events were observed.

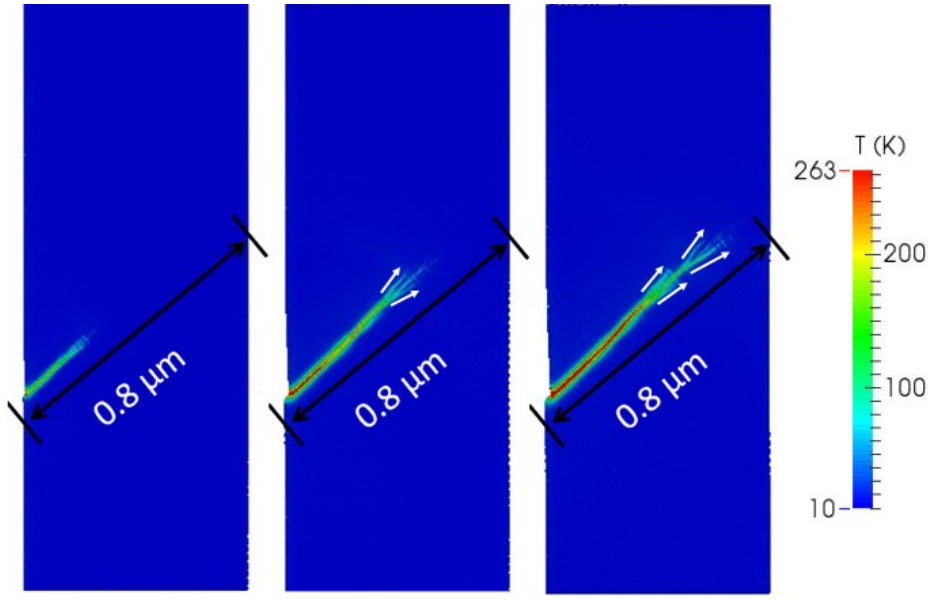

Fig. 6. Temperature distribution during shear band propagation showing shear band branching for the same sample analyzed in Fig. 4. The representative snapshots are taken at simulation running time of 0.3, 0.44, and 0.5 ns, respectively. The whole process of shear band propagation is available in Movie S1 in the Supplementary Material.

3.4. Propagation dynamics of multiple intersecting shear bands

Similar to dislocation intersections in which jogs/kinks may form that significantly affect plastic deformation of crystalline metals, shear bands may intersect in metallic glasses which could alter its mechanical behaviors [44,77,78]. For instance, Zhao [44] has studied the shear band interaction in compressive tests on specimens with two symmetrical semi-circular notches, and ascribed the observed 'work-hardening' behavior to stress interaction caused by stress fields around the shear band tips after quantitative analysis. It is therefore of scientific and practical

importance to investigate the dynamics of intersecting shear bands, which is challenging to observe experimentally in real time.

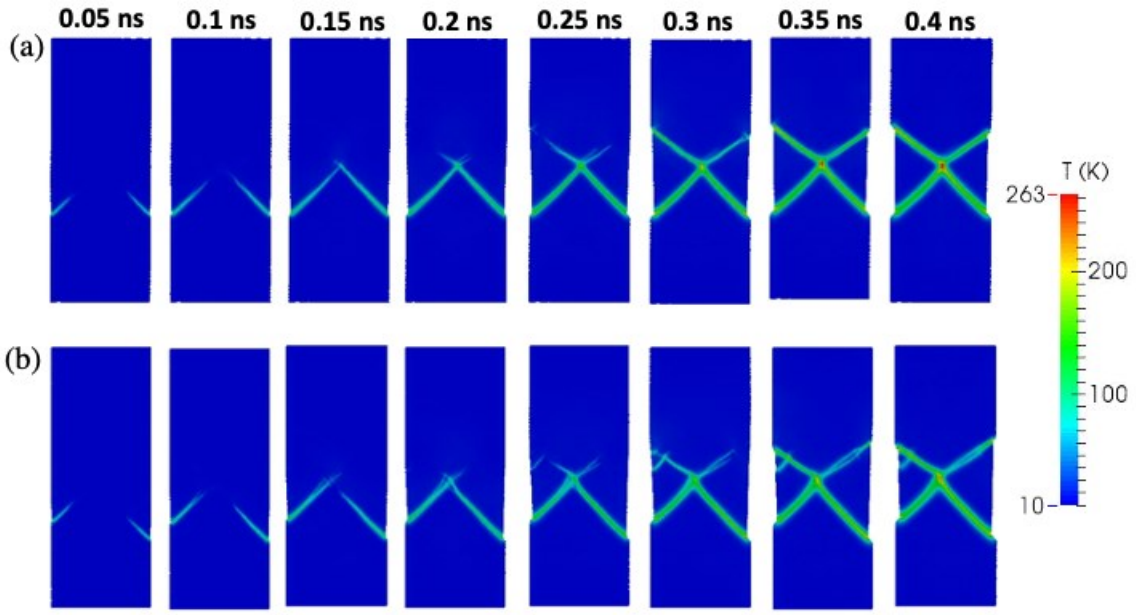

Fig. 7. Propagation evolution of two shear bands initiated symmetrically (a) and asymmetrically (b) from the two free surfaces of the LJ system with 4.5% prescribed uniaxial tensile strain traveling towards each other, crossing paths, and departing from each other afterwards. The snapshots are taken in an equal simulation running time interval of 0.05 ns.

Here, by using the PSL method, two incipient shear bands were nucleated on both sides of the LJ sample surface. The location of the incipient shear band was adjusted to achieve: (1) symmetric shear band intersection with roughly identical propagating distance, roughly in the middle of the sample; (2) asymmetric shear band intersection with different propagating distances, away from the middle of the sample. Fig. 7 shows the processes of both symmetric and asymmetric intersections. It can be clearly seen that the propagation of shear bands slows down noticeably upon approaching each other (more details in Movies S2 and S3 in the Supplementary Material).

In addition, the shear band propagation pathway gets deflected at the crossing junction, sometimes with branching. The slowdown, deflection and branching of shear band are all caused by the partially unloaded stress field ahead of the shear band. Lastly, the shear band intersection intensifies shear deformations and leads to further local heating at the junction. The temperature rise at the junction seems higher for symmetric intersection than asymmetric intersection. It should be noted that this temperature rise is due to sample gliding along shear bands, thus does not occur immediately upon shear band intersection.

Many of these observations echo the atomistic mechanisms of shear band interaction proposed by Sopu *et al*. [46] in which a $Cu_{64}Zr_{36}$ model metallic glass sample with two primary shear bands induced by symmetrical surface notches was loaded to closely look at the interaction. It was found that the shear bands interacted through elastic heterogeneities long before the plastic zones of two shear fronts started to intersect. Upon intersection of the shear bands, large stress fluctuations at the intersection point were induced, which in turn perturbed the STZ percolation process and, ultimately led to shear band branching and further multiplication.

4. Conclusions

To understand the dynamics of propagating shear band in metallic glasses, we conducted micron-scale MD simulations on two systems using distinctly different force fields. We made the following observations: (1) Driven by elastic energy stored in the sample, the average shear band propagation speed increases with increasing prescribed uniaxial tensile strain; (2) The instantaneous propagation speed keeps accelerating and could get close to or surpass the shear wave speed; (3) The shear strain singularity ahead of propagating shear band scales as $1/r$, which resembles typical cracks in brittle materials under the framework of weakly non-linear fracture

mechanics; (4) The propagation of shear band has intrinsic instability that manifests itself as microbranching and considerable fluctuations of instantaneous propagation speed; (5) Upon intersecting, shear bands can slow down, deflect, branch, and heat up locally. Our observations indicate that the dynamics of rapidly propagating shear band in metallic glasses can be viewed as shear cracks under the framework of weakly nonlinear fracture mechanics theory.

Declaration of Competing Interest

The authors declare that they have no known competing financial interests or personal relationships that could have appeared to influence the work reported in this paper.

Acknowledgements

We thank the support from the National Science Foundation of the United States under Grant DMR-1207439, DMR-1936368 and DMR-2015557, and the Center for Computational Innovations at Rensselaer Polytechnic Institute.

References

[1] C.A. Schuh, T.C. Hufnagel, U. Ramamurty, Mechanical behavior of amorphous alloys, Acta Mater. 55 (2007) 4067–4109. https://doi.org/10.1016/j.actamat.2007.01.052.
[2] W.H. Wang, C. Dong, C.H. Shek, Bulk metallic glasses, Mater. Sci. Eng. R Rep. 44 (2004) 45–89. https://doi.org/10.1016/j.mser.2004.03.001.
[3] J. Liu, N. Liu, M. Sun, J. Li, S. Sohn, J. Schroers, Fast Screening of Corrosion Trends in Metallic Glasses, ACS Comb. Sci. 21 (2019) 666–674. https://doi.org/10.1021/acscombsci.9b00073.
[4] W.L. Johnson, K. Samwer, A Universal Criterion for Plastic Yielding of Metallic Glasses with a (T/Tg)^2/3 Temperature Dependence, Phys. Rev. Lett. 95 (2005) 195501. https://doi.org/10.1103/PhysRevLett.95.195501.
[5] D. Jang, J.R. Greer, Transition from a strong-yet-brittle to a stronger-and-ductile state by size reduction of metallic glasses, Nat. Mater. 9 (2010) 215–219. https://doi.org/10.1038/nmat2622.
[6] L. Tian, Y.-Q. Cheng, Z.-W. Shan, J. Li, C.-C. Wang, X.-D. Han, J. Sun, E. Ma, Approaching the ideal elastic limit of metallic glasses, Nat. Commun. 3 (2012) 609. https://doi.org/10.1038/ncomms1619.
[7] J. Xu, E. Ma, Damage-tolerant Zr-Cu-Al-based bulk metallic glasses with record-breaking fracture toughness, J. Mater. Res. 29 (2014) 1489–1499. https://doi.org/10.1557/jmr.2014.160.
[8] M.D. Demetriou, M.E. Launey, G. Garrett, J.P. Schramm, D.C. Hofmann, W.L. Johnson, R.O. Ritchie, A damage-tolerant glass, Nat. Mater. 10 (2011) 123–128. https://doi.org/10.1038/nmat2930.

[9] A.L. Greer, Y.Q. Cheng, E. Ma, Shear bands in metallic glasses, Mater. Sci. Eng. R Rep. 74 (2013) 71–132. https://doi.org/10.1016/j.mser.2013.04.001.
[10] R. Maaß, J.F. Löffler, Shear-Band Dynamics in Metallic Glasses, Adv. Funct. Mater. 25 (2015) 2353–2368. https://doi.org/10.1002/adfm.201404223.
[11] M.L. Falk, J.S. Langer, Dynamics of viscoplastic deformation in amorphous solids, Phys. Rev. E. 57 (1998) 7192–7205. https://doi.org/10.1103/PhysRevE.57.7192.
[12] R.T. Qu, Z.Q. Liu, G. Wang, Z.F. Zhang, Progressive shear band propagation in metallic glasses under compression, Acta Mater. 91 (2015) 19–33. https://doi.org/10.1016/j.actamat.2015.03.026.
[13] A. Vinogradov, M. Seleznev, I.S. Yasnikov, Dislocation characteristics of shear bands in metallic glasses, Scr. Mater. 130 (2017) 138–142. https://doi.org/10.1016/j.scriptamat.2016.11.017.
[14] A.J. Cao, Y.Q. Cheng, E. Ma, Structural processes that initiate shear localization in metallic glass, Acta Mater. 57 (2009) 5146–5155. https://doi.org/10.1016/j.actamat.2009.07.016.
[15] E.R. Homer, Examining the initial stages of shear localization in amorphous metals, Acta Mater. 63 (2014) 44–53. https://doi.org/10.1016/j.actamat.2013.09.050.
[16] S.X. Song, T.G. Nieh, Direct measurements of shear band propagation in metallic glasses – An overview, Intermetallics. 19 (2011) 1968–1977. https://doi.org/10.1016/j.intermet.2011.06.018.
[17] W.J. Wright, R.R. Byer, X. Gu, High–speed imaging of a bulk metallic glass during uniaxial compression, Appl. Phys. Lett. 102 (2013) 241920. https://doi.org/10.1063/1.4811744.
[18] R. Dasgupta, H.G.E. Hentschel, I. Procaccia, Microscopic mechanism of shear bands in amorphous solids, Phys. Rev. Lett. 109 (2012) 255502. https://doi.org/10.1103/PhysRevLett.109.255502.
[19] C.E. Maloney, A. Lemaître, Amorphous systems in athermal, quasistatic shear, Phys. Rev. E. 74 (2006) 016118. https://doi.org/10.1103/PhysRevE.74.016118.
[20] F. Shimizu, S. Ogata, J. Li, Theory of Shear Banding in Metallic Glasses and Molecular Dynamics Calculations, Mater. Trans. 48 (2007) 2923–2927. https://doi.org/10.2320/matertrans.MJ200769.
[21] D. Srolovitz, V. Vitek, T. Egami, An atomistic study of deformation of amorphous metals, Acta Metall. 31 (1983) 335–352. https://doi.org/10.1016/0001-6160(83)90110-4.
[22] S. Takeuchi, K. Edagawa, Atomistic simulation and modeling of localized shear deformation in metallic glasses, Prog. Mater. Sci. 56 (2011) 785–816. https://doi.org/10.1016/j.pmatsci.2011.01.007.
[23] D. Şopu, A. Stukowski, M. Stoica, S. Scudino, Atomic-Level Processes of Shear Band Nucleation in Metallic Glasses, Phys. Rev. Lett. 119 (2017) 195503. https://doi.org/10.1103/PhysRevLett.119.195503.
[24] H. Sheng, D. Şopu, S. Fellner, J. Eckert, C. Gammer, Mapping Shear Bands in Metallic Glasses: From Atomic Structure to Bulk Dynamics, Phys. Rev. Lett. 128 (2022) 245501. https://doi.org/10.1103/PhysRevLett.128.245501.
[25] G. Wahnström, Molecular-dynamics study of a supercooled two-component Lennard-Jones system, Phys. Rev. A. 44 (1991) 3752–3764. https://doi.org/10.1103/PhysRevA.44.3752.
[26] Y.Q. Cheng, E. Ma, H.W. Sheng, Atomic Level Structure in Multicomponent Bulk Metallic Glass, Phys. Rev. Lett. 102 (2009) 245501. https://doi.org/10.1103/PhysRevLett.102.245501.
[27] J. Luo, Y. Shi, The local stress state of a running shear band in amorphous solids, J. Mater. Res. 30 (2015) 1979–1987. https://doi.org/10.1557/jmr.2015.141.
[28] J. Luo, Y. Shi, Tensile fracture of metallic glasses via shear band cavitation, Acta Mater. 82 (2015) 483–490. https://doi.org/10.1016/j.actamat.2014.09.008.
[29] E. Bouchbinder, A. Livne, J. Fineberg, The 1/r singularity in weakly nonlinear fracture mechanics, J. Mech. Phys. Solids. 57 (2009) 1568–1577. https://doi.org/10.1016/j.jmps.2009.05.006.
[30] E. Bouchbinder, A. Livne, J. Fineberg, Weakly nonlinear fracture mechanics: experiments and theory, Int. J. Fract. 162 (2010) 3–20. https://doi.org/10.1007/s10704-009-9427-3.
[31] Y. Shi, M.L. Falk, Structural transformation and localization during simulated nanoindentation of a noncrystalline metal film, Appl. Phys. Lett. 86 (2005) 011914. https://doi.org/10.1063/1.1844593.
[32] Y.Q. Cheng, E. Ma, H.W. Sheng, Atomic Level Structure in Multicomponent Bulk Metallic Glass, Phys. Rev. Lett. 102 (2009) 245501. https://doi.org/10.1103/PhysRevLett.102.245501.
[33] Y.Q. Cheng, E. Ma, Configurational dependence of elastic modulus of metallic glass, Phys. Rev. B. 80 (2009) 064104. https://doi.org/10.1103/PhysRevB.80.064104.

[34] S. Plimpton, Fast Parallel Algorithms for Short-Range Molecular Dynamics, J. Comput. Phys. 117 (1995) 1–19. https://doi.org/10.1006/jcph.1995.1039.
[35] S. Nosé, A unified formulation of the constant temperature molecular dynamics methods, J. Chem. Phys. 81 (1984) 511–519. https://doi.org/10.1063/1.447334.
[36] W.G. Hoover, Canonical dynamics: Equilibrium phase-space distributions, Phys. Rev. A. 31 (1985) 1695–1697. https://doi.org/10.1103/PhysRevA.31.1695.
[37] Y. Shi, J. Luo, F. Yuan, L. Huang, Intrinsic ductility of glassy solids, J. Appl. Phys. 115 (2014) 043528. https://doi.org/10.1063/1.4862959.
[38] K. Albe, Y. Ritter, D. Şopu, Enhancing the plasticity of metallic glasses: Shear band formation, nanocomposites and nanoglasses investigated by molecular dynamics simulations, Mech. Mater. 67 (2013) 94–103. https://doi.org/10.1016/j.mechmat.2013.06.004.
[39] X. Yuan, D. Şopu, F. Moitzi, K.K. Song, J. Eckert, Intrinsic and extrinsic effects on the brittle-to-ductile transition in metallic glasses, J. Appl. Phys. 128 (2020) 125102. https://doi.org/10.1063/5.0020201.
[40] Y. Shi, M.L. Falk, Strain Localization and Percolation of Stable Structure in Amorphous Solids, Phys. Rev. Lett. 95 (2005) 095502. https://doi.org/10.1103/PhysRevLett.95.095502.
[41] Y. Shi, M.B. Katz, H. Li, M.L. Falk, Evaluation of the Disorder Temperature and Free-Volume Formalisms via Simulations of Shear Banding in Amorphous Solids, Phys. Rev. Lett. 98 (2007) 185505. https://doi.org/10.1103/PhysRevLett.98.185505.
[42] Y. Shi, M.L. Falk, Atomic-scale simulations of strain localization in three-dimensional model amorphous solids, Phys. Rev. B. 73 (2006) 214201. https://doi.org/10.1103/PhysRevB.73.214201.
[43] J.Q. Wang, J.H. Perepezko, Focus: Nucleation kinetics of shear bands in metallic glass, J. Chem. Phys. 145 (2016) 211803. https://doi.org/10.1063/1.4966662.
[44] J.X. Zhao, Understanding the shear band interaction in metallic glass, Philos. Mag. Lett. 96 (2016) 35–43. https://doi.org/10.1080/09500839.2015.1134834.
[45] D. Şopu, S. Scudino, X.L. Bian, C. Gammer, J. Eckert, Atomic-scale origin of shear band multiplication in heterogeneous metallic glasses, Scr. Mater. 178 (2020) 57–61. https://doi.org/10.1016/j.scriptamat.2019.11.006.
[46] D. Şopu, F. Moitzi, N. Mousseau, J. Eckert, An atomic-level perspective of shear band formation and interaction in monolithic metallic glasses, Appl. Mater. Today. 21 (2020) 100828. https://doi.org/10.1016/j.apmt.2020.100828.
[47] J. Luo, Y. Shi, C.R. Picu, Shear-induced volumetric strain in CuZr metallic glass, Int. J. Eng. Sci. 83 (2014) 99–106. https://doi.org/10.1016/j.ijengsci.2014.04.009.
[48] F. Shimizu, S. Ogata, J. Li, Yield point of metallic glass, Acta Mater. 54 (2006) 4293–4298. https://doi.org/10.1016/j.actamat.2006.05.024.
[49] A. Livne, G. Cohen, O. Ben-David, J. Fineberg, Universal Aspects of Dynamic Fracture in Brittle Materials, AIP Conf. Proc. 742 (2004) 122–131. https://doi.org/10.1063/1.1846468.
[50] A. Livne, O. Ben-David, J. Fineberg, Oscillations in Rapid Fracture, Phys. Rev. Lett. 98 (2007) 124301. https://doi.org/10.1103/PhysRevLett.98.124301.
[51] T.C. Hufnagel, C.A. Schuh, M.L. Falk, Deformation of metallic glasses: Recent developments in theory, simulations, and experiments, Acta Mater. 109 (2016) 375–393. https://doi.org/10.1016/j.actamat.2016.01.049.
[52] A.A. Long, W.J. Wright, X. Gu, A. Thackray, M. Nakib, J.T. Uhl, K.A. Dahmen, Experimental evidence that shear bands in metallic glasses nucleate like cracks, Sci. Rep. 12 (2022) 18499. https://doi.org/10.1038/s41598-022-22548-8.
[53] J.D. Eshelby, Uniformly Moving Dislocations, Proc. Phys. Soc. Sect. A. 62 (1949) 307. https://doi.org/10.1088/0370-1298/62/5/307.
[54] L.B. Freund, Dynamic Fracture Mechanics, Cambridge University Press, Cambridge, 1990. https://doi.org/10.1017/CBO9780511546761.
[55] F.F. Abraham, H. Gao, How Fast Can Cracks Propagate?, Phys. Rev. Lett. 84 (2000) 3113–3116. https://doi.org/10.1103/PhysRevLett.84.3113.

[56] null Rosakis, null Samudrala, null Coker, Cracks faster than the shear wave speed, Science. 284 (1999) 1337–1340. https://doi.org/10.1126/science.284.5418.1337.
[57] E. Faran, D. Shilo, Twin motion faster than the speed of sound, Phys. Rev. Lett. 104 (2010) 155501. https://doi.org/10.1103/PhysRevLett.104.155501.
[58] P. Rosakis, H. Tsai, Dynamic twinning processes in crystals, Int. J. Solids Struct. 32 (1995) 2711–2723. https://doi.org/10.1016/0020-7683(94)00293-6.
[59] null Rosakis, Supersonic Dislocation Kinetics from an Augmented Peierls Model, Phys. Rev. Lett. 86 (2001) 95–98. https://doi.org/10.1103/PhysRevLett.86.95.
[60] null Gumbsch, null Gao, Dislocations faster than the speed of sound, Science. 283 (1999) 965–968. https://doi.org/10.1126/science.283.5404.965.
[61] V. Nosenko, S. Zhdanov, G. Morfill, Supersonic dislocations observed in a plasma crystal, Phys. Rev. Lett. 99 (2007) 025002. https://doi.org/10.1103/PhysRevLett.99.025002.
[62] K. Xia, A.J. Rosakis, H. Kanamori, Laboratory Earthquakes: The Sub-Rayleigh-to-Supershear Rupture Transition, Science. 303 (2004) 1859–1861. https://doi.org/10.1126/science.1094022.
[63] A. Livne, E. Bouchbinder, J. Fineberg, Breakdown of Linear Elastic Fracture Mechanics near the Tip of a Rapid Crack, Phys. Rev. Lett. 101 (2008). https://doi.org/10.1103/PhysRevLett.101.264301.
[64] A. Livne, E. Bouchbinder, I. Svetlizky, J. Fineberg, The Near-Tip Fields of Fast Cracks, Science. 327 (2010) 1359–1363. https://doi.org/10.1126/science.1180476.
[65] J. Luo, P. Keblinski, Y. Shi, A model metallic glass exhibits size-independent tensile ductility, Acta Mater. 103 (2016) 587–594. https://doi.org/10.1016/j.actamat.2015.10.029.
[66] B. Deng, Y. Shi, On measuring the fracture energy of model metallic glasses, J. Appl. Phys. 124 (2018) 035101. https://doi.org/10.1063/1.5037352.
[67] F.-F. Wu, K.C. Chan, S.-S. Jiang, S.-H. Chen, G. Wang, Bulk metallic glass composite with good tensile ductility, high strength and large elastic strain limit, Sci. Rep. 4 (2014) 5302. https://doi.org/10.1038/srep05302.
[68] J. Luo, B. Deng, K.D. Vargheese, A. Tandia, S.E. DeMartino, J.C. Mauro, Atomic-scale modeling of crack branching in oxide glass, Acta Mater. 216 (2021) 117098. https://doi.org/10.1016/j.actamat.2021.117098.
[69] A. Livne, O. Ben-David, J. Fineberg, Oscillations in Rapid Fracture, Phys. Rev. Lett. 98 (2007). https://doi.org/10.1103/PhysRevLett.98.124301.
[70] F. Abraham, H. Gao, How Fast Can Cracks Propagate?, Phys. Rev. Lett. 84 (2000) 3113–3116. https://doi.org/10.1103/PhysRevLett.84.3113.
[71] A.J. Rosakis, Cracks Faster than the Shear Wave Speed, Science. 284 (1999) 1337–1340. https://doi.org/10.1126/science.284.5418.1337.
[72] J. Fineberg, E. Bouchbinder, Recent developments in dynamic fracture: some perspectives, Int. J. Fract. 196 (2015) 33–57. https://doi.org/10.1007/s10704-015-0038-x.
[73] E. Bouchbinder, T. Goldman, J. Fineberg, The dynamics of rapid fracture: instabilities, nonlinearities and length scales, Rep. Prog. Phys. 77 (2014) 046501. https://doi.org/10.1088/0034-4885/77/4/046501.
[74] M. Marder, S. Gross, Origin of crack tip instabilities, J. Mech. Phys. Solids. 43 (1995) 1–48. https://doi.org/10.1016/0022-5096(94)00060-I.
[75] H. Gao, Surface roughening and branching instabilities in dynamic fracture, J. Mech. Phys. Solids. 41 (1993) 457–486. https://doi.org/10.1016/0022-5096(93)90044-G.
[76] X. Yuan, D. Şopu, J. Eckert, Origin of strain hardening in monolithic metallic glasses, Phys. Rev. B. 103 (2021) L140107. https://doi.org/10.1103/PhysRevB.103.L140107.
[77] D.P. Wang, B.A. Sun, X.R. Niu, Y. Yang, W.H. Wang, C.T. Liu, Mutual interaction of shear bands in metallic glasses, Intermetallics. 85 (2017) 48–53. https://doi.org/10.1016/j.intermet.2017.01.015.
[78] K.E. Avila, S. Küchemann, H.M. Urbassek, Interaction between parallel shear bands in a metallic glass, J. Non-Cryst. Solids. 566 (2021) 120882. https://doi.org/10.1016/j.jnoncrysol.2021.120882.